RESEARCH ARTICLE OPEN ACCESS

# Macrophage Changes and High-Throughput Sequencing in Aging Mouse Intervertebral Disks

Wei Wang[1,2] | Cheng Jiang[2,3] | Jiong-Hui Chen[2,3] | Yong-Long Chen[2,3] | Zhen-Wu Zhang[2,3] | Zhi-Chao Yang[2,3] | Jun Li[2,3] | Xiao-Chuan Li[2]

[1]Chongqing Tongnan Hospital of Traditional Chinese Medicine, Chongqing, People's Republic of China | [2]Department of Orthopaedic Surgery, Gaozhou People's Hospital, Gaozhou, Guangdong Province, People's Republic of China | [3]Graduate School of Guangdong Medical University, ZhanJiang, Guangdong, People's Republic of China

**Correspondence:** Xiao-Chuan Li (lixcgzph@163.com)

**Received:** 17 December 2024 | **Revised:** 10 March 2025 | **Accepted:** 12 March 2025

**Funding:** This work was supported by Guangdong Medical Research Fund (B2023375, B2024310), Guangdong Province Traditional Chinese Medicine Research Project (20241380), and Natural Science Foundation of Guangdong Province (2024A1515013042).

**Keywords:** high-throughput sequencing | intervertebral disk | macrophages | senescence

## ABSTRACT

**Background:** Intervertebral disk (IVD) degeneration is associated with lower back pain and aging; however, the mechanisms underlying age-related changes and the changes in macrophage polarization in aging intervertebral disks require further elucidation. The aim of this study was to evaluate changes in macrophages, the differential expression of senescence genes, and their relationship with hub genes in IVDs during aging in mice.

**Methods:** Twenty-eight male wild C57 mice aged 4 weeks were divided into two groups. Four mice per group were selected for high-throughput sequencing and 10 for tail IVD immunohistochemical analysis. Adult and aged mouse IVD specimens were stained with hematoxylin–eosin, Fast Green, and Alcian Blue to determine collagen (Col) 1, Col2, proteoglycan, P16, P21, P53, CD11b, CD86, CD206, IL-1, TGF-β, and IL-4 expression. High-throughput sequencing was performed on adult and aged mouse IVD tissues.

**Results:** Aged mouse IVDs showed reduced height and marked degeneration, with decreased Col2 and proteoglycan expression and increased Col1 expression. The expression of senescence markers, senescence-associated IL-1, TGF-β, and IL-4, and macrophage-related markers, CD11b, CD86, and CD206, increased markedly with age. High-throughput sequencing revealed 1975 differentially expressed genes in adult and aged mice, with 797 genes showing upregulated expression (top five: *Kcna7*, *Mmp9*, *Panx3*, *Myl10*, and *Bglap*) and 1178 showing downregulated expression (top five: *Srd5a2*, *Slc38a5*, *Gm47283*, *Npy*, and *Pcdh8*). Gene Ontology and pathway enrichment analyses highlighted aging-related cellular components, biological processes, and metabolic pathways. The identified hub genes included *Cox5a*, *Ndufs6*, and *Ndufb9*.

**Conclusions:** Disk senescence and reduced height in aged mice are linked to upregulated expression of senescence-associated phenotypes and macrophage polarization markers. These findings suggest that macrophages and differential gene expression play key roles in age-related IVD degeneration, indicating that they can be used as potential targets for therapeutic intervention.

## 1 | Introduction

Persistent lower back pain (LBP) is the most common chronic condition, the second leading cause of medical visits, and a major contributor to physical disability [1]. Up to 80% of people experience LBP during their lifetime [2]. The incidence and prevalence of LBP have increased rapidly, even in young people. Over 40% of adolescents have experienced LBP of varying degrees in the last year [3–5]. Intervertebral disk (IVD) degeneration is associated with LBP, with age being a key contributor [6]. Current treatment strategies, including conservative treatment and surgical intervention, aim at providing symptomatic relief but do not target the underlying pathogenesis [7]. Additionally, IVD degeneration is associated with an increase in inflammation. Macrophages play different roles in IVD degeneration. They infiltrate degenerated IVDs in humans and rodents, especially in the completely enclosed nucleus pulposus region, exacerbating disk degeneration [8–10].

IVD degeneration refers to the structural and functional deterioration of the IVD due to abnormal pathological changes in cells and the extracellular matrix (ECM). It may be caused by genetic predisposition, injury, aging, smoking, and other environmental factors or any combination thereof. While injury or genetic defects are common causes of IVD degeneration in young individuals [11–13], disk aging is a systemic process and occurs in all IVDs in older people. Senescence is an irreversible process of halted cell proliferation and a complex, dynamic, and a multistep process. It is triggered by telomere shortening, stress-induced DNA damage accumulation, and other types of cellular stress. To identify senescence, multiple biomarkers are used, including increased expression of cell cycle regulatory kinases such as p16, p21, and p53 [14].

Despite finding evidence of disk degeneration in younger, relatively healthy individuals, no signs of aging have been observed; moreover, the differences between senescence and degenerated disks are not clearly defined, as both appear to be characterized by similar changes [15]. Therefore, studies to determine the common characteristics of aging and degeneration that affect IVD function are crucial for guiding new treatments.

Similar to other cell types, cells of IVDs may be susceptible to senescence, which may be involved in the pathogenesis of age-related IVD degeneration. However, comprehensive systematic studies on cellular senescence in mouse IVDs are lacking. Therefore, in this study, we aimed to evaluate caudal IVD specimens from adult and older mice to study M0, M1, and M2 macrophage polarization and their aging-related secretory phenotypes. Additionally, we aimed to assess macrophage polarization in aged disks, along with the differential expression of genes related to aging, and the hub genes involved in aging. We believe that our observations could provide important experimental evidence regarding macrophage changes in aged IVDs and offer new information on the pathogenesis of age-triggered disk degeneration diseases.

## 2 | Materials and Methods

### 2.1 | Collection of Mouse IVD Tissues

This animal study protocol and procedures were ethically reviewed and approved by the Ethics Committee of Gaozhou People's Hospital (No. GYLLPJ-2021024). Twenty-eight 2-month-old male wild C57 mice were purchased from the Guangdong Animal Experiment Center. The animals were maintained in a ventilated environment with a 12:12-h light–dark cycle at a constant temperature of 22°C. The mice were divided equally into two groups. The animals were subjected to complete digital radiography (DR) after being sacrificed via intraperitoneal injection of chloral hydrate at 2 and 24 months of age and measured the intervertebral disk height (DHI) of each mouse separately. To reduce errors, we measured the DHI, defined as the distance between high-density images above and below the intervertebral disk, three times on DR images of each intervertebral disk and took the average value. The 5th–7th caudal IVDs were removed: 4 of them were frozen at −80°C and 10 were fixed using 4% paraformaldehyde for 24 h followed by decalcification using 10% ethylene diamine tetra acetic acid for 2–3 months. This work has been reported in accordance with the Animal Research: Reporting of In Vivo Experiments (ARRIVE) guidelines [16].

### 2.2 | Histological Examination of Mouse IVD Specimens

After decalcification, the specimens were washed with phosphate-buffered saline, dehydrated using an ethanol gradient, and embedded in paraffin. The tissue wax blocks were sectioned into 5-μm-thick slices, baked in an oven at 60°C for 1.5 h, deparaffinized, and stained with hematoxylin and eosin (HE), Fast Green, and Alcian Blue.

### 2.3 | Immunohistochemical Staining

The tissue sections were immersed in 1× citrate buffer at 60°C for over 16 h. After blocking with endogenous peroxidase, the sections were incubated with goat serum. Next, the primary antibodies (dilutions: CD206 [1/300; 43920S; Cell Signaling, Boston, MA, USA]; CD11b [3/1000; 85 601; Cell Signaling]; CD86 [1/1000; 26 903-1-AP; Proteintech, Wuhan, China]; P16 [1/1000; 220 800; Abcam, Cambridge, MA, USA]; P21 [1/1000; 28 248-1-AP; Proteintech]; P53 [1/1000; 60 283-2-Ig; Proteintech]; Agg [1/500; 13 880-1-AP; Proteintech]; type I collagen [col 1] [1/1000; 14 695-1-AP; Proteintech]; type II collagen [col 2] [1/2000; 28 459-1-AP; Proteintech]; transforming growth factor beta [TGF-β] [1/800; 21 898-1-AP; Proteintech]; interleukin [IL]-1 [1/500; 16 765-1-AP; Proteintech]; and IL-4 [1/500; 66 142-1-Ig; Proteintech] were added, and the samples were incubated overnight at 4°C. After washing, the sections were incubated with secondary antibodies corresponding to the species of the primary antibodies used (rabbit anti-goat or mouse anti-goat) for 1 h at 37°C. Diaminobenzidine (DAB) was used for visualization, followed by nuclear counterstaining.

### 2.4 | High-Throughput Sequencing

The frozen IVDs from 2- and 24-month-old mice (four mice each) were subjected to high-throughput sequencing. Total RNA was isolated and purified using the TRIzol Reagent (Cat#15596–026, Thermo Fisher, USA) according to the manufacturer's instructions. To ensure high-quality total RNA for mRNA sequencing, its integrity was assessed using an Agilent 2100 BioAnalyzer with selection criteria of RIN ≥ 7 and a ribosomal RNA (rRNA) ratio of 28S/18S ≥ 1.5:1. The starting amount ranged from 0.1 to 1 μg. The initial total RNA was accurately quantified using the QUBIT RNA Assay Kit (Cat#Q10211, Thermo Fisher, USA). One sample with suboptimal RNA quality from each group was excluded during sample preparation. Library preparation and RNAseq were conducted at CapitalBio Technology (Beijing, China; www.capitalbiotech.com). Library preparation followed the NEBNext Ultra RNA Library Prep Kit for Illumina User Guide (Cat #E7530S/L, NEB, California, USA).

Briefly, the RNA library was prepared by the fragmentation of dscDNA, performing end repair to generate blunt ends, and adaptor ligation. The molar concentration of the constructed library was performed using q-PCR with the Illumina-recommended KAPA Quantification Kit (Cat#CK4602, Kapa Biosystems, Boston, USA). Equimolar amounts of each library were pooled and used for cluster generation on the cBot with the Illumina TruSeq PE Cluster Kit v3. The sequencing run was performed on a HiSeq 1000 instrument using the indexed, 2 × 100 cycles paired end (PE) protocol and the TruSeq SBS v3 Reagents according to the Illumina HiSeq 1000 System User Guide. Image analysis and base calling resulted in .bcl files, which were converted into .fastq files with the bcl2fastq v2.18 software.

The raw image files from Illumina high-throughput sequencing were base-called and converted into raw sequencing reads for subsequent analyses. The raw sequencing reads were processed to remove low-quality data. Filtering steps included: removing contaminant sequences and adapter sequences, truncating reads with an average base mass of less than 15 at both ends of the window (using a sliding window of four base lengths), removing reads with high N content (if the N content exceeds 5%, the entire read is removed), removing reads with more than 30% low-quality bases (score < 20), removing non-paired reads, and discarding reads shorter than 100 bp after trimming. After filtering, the Q30 score was greater than 93%, and the Q20 score exceeded 97% for all samples. Clean reads were aligned to the reference genome with an overall alignment rate exceeding 92%, while the multiple alignment rate is less than 8%.

For statistical analysis and the assessment of differential expression, an empirical Bayes method in *limma* was employed to moderate the standard errors of the estimated log2-fold changes. The moderated t-statistic was applied to each probe and contrast, generating *p*-values similar to ordinary *t*-statistics but with increased degrees of freedom for greater reliability. The *limma* functions topTable and decideTests were used to summarize the results, perform hypothesis testing, and adjust *p*-values for multiple testing. The results obtained include log2-fold changes, standard errors, *t*-statistics, and *p*-values [17].Log|2(fold change)| > 1 and $p \leq 0.05$ were set as the cut-offs to screen out differentially expressed gene (DEG) (If the comparison group contains multiple samples, then at least two thirds of the samples in the case or control group have gene expression in at least one of the groups, or at least two-thirds of the samples in the case/control group have expression and the average value is ≥ 1).

To explore the biological significance of DEGs and identify disturbed biological functions in IVD, we performed Gene Ontology Consortium (GO) classification. GO analysis categorized DEGs into biological processes, cellular components, and molecular functions. Functional enrichment analysis was performed for differentially expressed genes (DEGs) using the Database for Annotation, Visualization, and Integrated Discovery (GO: http://www.geneontology.org/) with a threshold of $p < 0.05$ [18]. GO terms with an adjusted *p* value < 0.05, as calculated by the hypergeometric test followed by the Benjamini–Hochberg method, were defined as significantly enriched terms. GO provides a comprehensive set of functional annotation tools for the investigation of the biological context of large lists of genes. Hierarchical clustering analysis was performed to group DEGs with similar expression patterns.

In our study, Kyoto Encyclopedia of Genes and Genomes (KEGG) pathway enrichment analysis was performed to determine the function of DEGs using KOBAS 2.0 (KEGG: http://www.genome.jp/kegg) with a threshold of $p < 0.05$. The top 30 terms with the lowest corrected *p*-values were selected to generate an enrichment pathway diagram. The STRING database (https://cn.string-db.org/), integrated as a Cytoscape plugin, was used to determine significantly overrepresented GO terms in the gene set. In STRING, if the combined score between two genes or proteins exceeded the defined threshold and both exhibited significant differences between groups, the gene or protein pair was extracted for further analysis.

### 2.5 | Statistical Analysis

The immunohistochemical results of the mouse IVDs were quantified using the ImageJ software (Java 1.8.0–172) and analyzed using GraphPad Prism 9.0. We determined the upper and lower endplates, annulus fibrosus, and nucleus pulposus of each intervertebral disk as distinct regions. The threshold was adjusted in ImageJ to ensure that the stained area closely matched the actual stained region. To minimize errors, three independent researchers analyzed each intervertebral disk, and the average value was recorded. The data were analyzed using non-paired *t*-tests for comparisons and graphing. Results with $p < 0.05$ were considered statistically significant.

## 3 | Results

### 3.1 | Decreased Height and Increased Degeneration of Aged Mouse IVDs

Disk height analyses of mouse caudal spine radiographs revealed that the heights of the caudal spine disks in senescent mice were lower than those in adult mice ($p < 0.05$, $t = 2.17$, Figure 1B,C). Histological examination of the aged mouse IVDs using HE, Fast Green, and Alcian Blue showed a decrease in the number of nucleus pulposus cells, matrix thinning after substantial

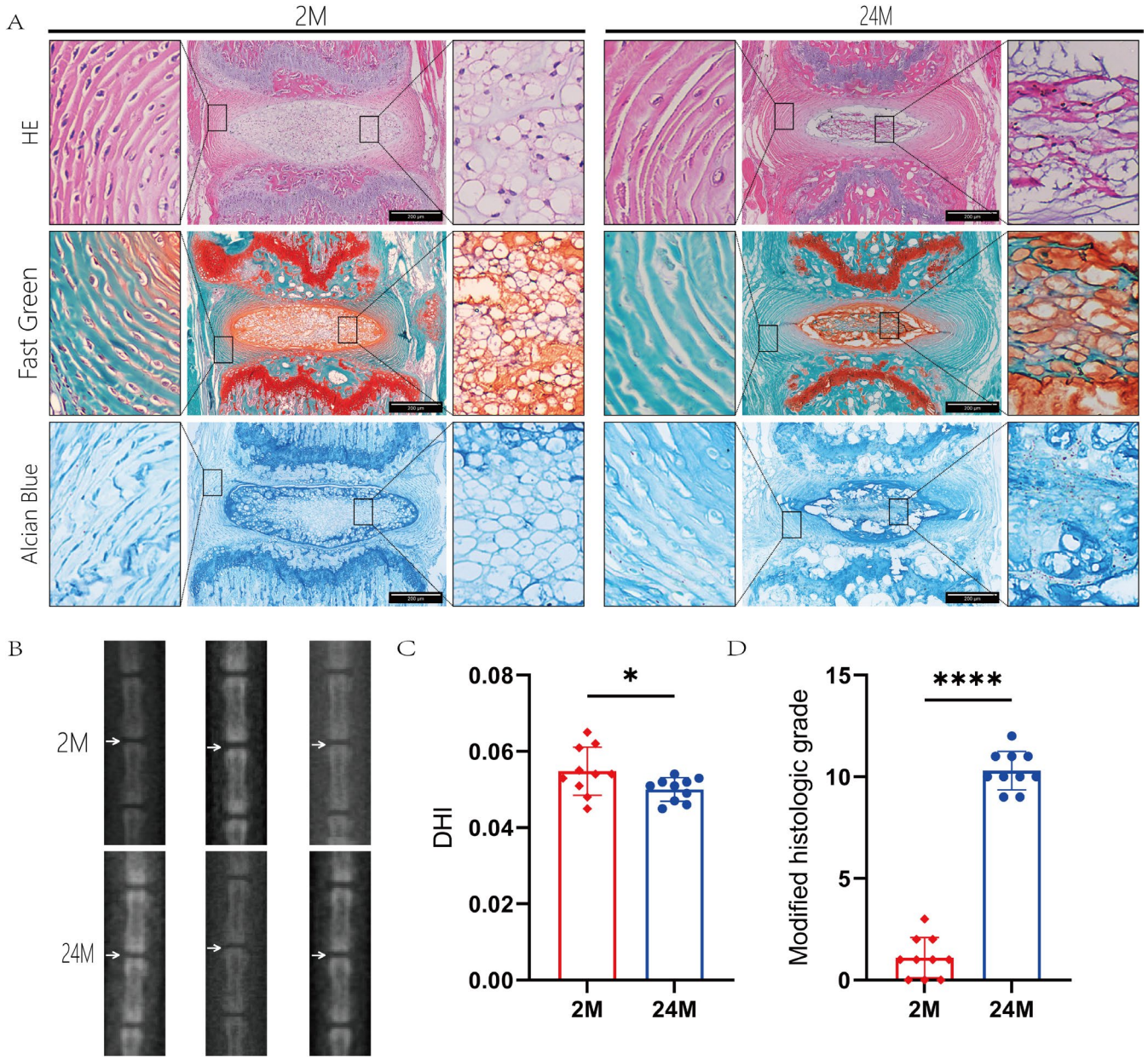


**FIGURE 1** | | Mouse IVD images showing tissue staining and DR showing the disk height statistics. (A) Saffron O, Fast Green, and Alcian Blue staining (scale bar: 200 μm, magnification ×10); (B, C) DR and caudal vertebrae of adult and aged mice and height statistics; (D) IVD altered histological scoring statistic (*$p < 0.05$, ****$p < 0.0001$). Each point on the statistical chart represents a mouse.

loss of aggregated proteoglycan, reduction in the size of round cells, increase in the number of stellate cells, arrangement in cell clusters, separation of cells into strips of aggregated proteoglycan (Agg) matrix, absence of notochord cells, appearance of protuberances and torn and disorganized lamellae of the annulus, and a significant increase in the chondrocyte proportion in the annulus. The proportion of chondrocytes in the fiber ring increased significantly and the boundary between the nucleus pulposus and the fiber ring was severely disrupted (Figure 1A). Quantification of the degree of IVD degeneration in the two groups of mice using modified histological scores [19] showed that the histological scores of IVDs in aged mice were significantly higher than those in adult mice. DR showed a reduction in disk height. These findings indicated severe degeneration of the caudal disks in aged mice ($p < 0.0001$, $t = 19.29$, Figure 1D).

### 3.2 | Increased Expression of Senescence Biomarkers and Imbalance in ECM Metabolism in Aging Mouse IVDs

In humans, rats, and mouse models of accelerated aging, the number of senescent IVD cells increases with age. However, whether cellular senescence occurs in the IVDs of naturally aging mice is not understood. Therefore, we assessed the expression of three key senescence biomarkers, P16, P21, and P53 [20], in the caudal intervertebral tissue sections collected from 10 mice aged 2 months and 10 mice aged 24 months; cyclin-dependent kinase inhibitors were used to promote cell growth arrest and senescence to verify the aging condition of IVDs in older mice. The results showed that the proportion of cells that stained positively for P16 ($p < 0.0001$, $t = 19.39$), P21 ($p < 0.0001$,

$t = 20.48$), and P53 ($p < 0.0001$, $t = 44.69$) (Figure 2) was significantly higher in the aged mouse IVD tissue than in adult mouse tissue.

Imbalance in matrix homeostasis, particularly the reduced synthesis and metabolism of ECM collagen and Agg and enhanced degradation, is a key sign of age-related IVD degeneration [21]. We performed immunohistochemical staining for Col1, Col2, and Agg in adult and aged mouse tissues to verify IVD degeneration in aged mice. Compared with those in adult mice, the expression of Col2 ($p < 0.0001$, $t = 12.44$) and Agg ($p < 0.001$, $t = 4.708$) in the aged mouse IVDs reduced significantly, whereas that of Col1 ($p < 0.01$, $t = 3.334$) increased (Figure 2), confirming the severe imbalance in matrix metabolism and degeneration in older mouse IVDs.

### 3.3 | Elevated Expression of Macrophage Markers and Senescence-Associated Inflammatory Factors in IVDs of Aging Mice

We performed immunohistochemical staining for macrophage-related phenotypes in adult and aged mouse tissues to understand macrophage polarization in mouse IVDs. M0-type macrophages express CD11b, the pro-inflammatory M1 subtype is characterized by CD86 expression, while the anti-inflammatory M2 subtype is represented by the CD206 marker [22–24]. In the aged mouse IVDs, the expression of these macrophage markers (CD11b ($p < 0.0001$, $t = 20.79$), CD86 ($p < 0.0001$, $t = 8.419$), CD206 ($p < 0.0001$, $t = 5.803$)) was significantly higher than that in adult tissues.

The senescence-associated secretory phenotype (SASP) is a key mediator of senescence-induced degenerative phenotypes; while IL-1 triggers SASP activation, TGF-β contributes to the senescent phenotype and the pro-inflammatory IL-4 is associated with M2 macrophage activation [25–27]. Therefore, immunohistochemical staining was performed for IL-1, IL-4, and TGF-β in adult and aged mouse IVD tissues to verify the presence of SASP components. The expression of IL-1 ($p < 0.01$, $t = 3.848$) and TGF-β ($p < 0.01$, $t = 3.306$) in the aged caudal IVDs was significantly higher than that in the caudal IVDs of adult mice; the IL-4 ($p < 0.05$, $t = 2.448$) level also increased in the IVDs (Figure 3).

### 3.4 | Differential Gene Expression in Aging Mouse IVDs

Differential expression analyses with biological replicates or pairs were performed using the R *limma* package, and comparisons without biological replicates were performed using the DESeq package. $|\log2FC| \geq 1$ and $p \leq 0.05$ were used as DEG screening criteria.

In total, 1975 DEGs were identified; the expression of 797 DEGs was upregulated, with *Srd5a2*, *Slc38a5*, *Gm47283*, *Npy*, and *Pcdh8* being the top five (Table 1), while the expression of 1178 DEGs was downregulated, with *Kcna7*, *Mmp9*, *Panx3*, *Myl10*, and *Bglap* being the top five (Table 2). The volcano plot in Figure 4A shows the differential expression of genes. Hierarchical cluster analysis was performed on DEGs, and genes with the same or similar expression patterns were clustered (Figure 4B).

### 3.5 | GO and Pathway Analyses of DEGs in the IVDs of Aged Mice

The DEGs were mapped to each entry of the GO database, the number of genes in each entry was calculated, and *p*-values were obtained from hypothesis testing using hypergeometric distribution. The *p*-values were corrected to reduce the number of false positives; the lower the corrected *p*-value, the more significant the enrichment results. Finally, the top 30 enriched GO terms were counted; enrichment was observed in biological processes (BP) and cellular components (CCs), but not in molecular functions (Figure 5A). Regarding CCs, the DEGs were mainly associated with contractile fibers (GO:0043292), myogenic fibers (GO:0030016), contractile fiber portions (GO:0044449), and myonectoderms (GO:0030017). In terms of BPs, the DEGs were associated with muscle contraction (GO:0006936), muscular systemic processes (GO:0003012), and muscle architecture development (GO:0061061).

The pathway enrichment analysis (Figure 5B) showed that DEGs in adult and aged mouse disks were mainly involved in metabolic pathways associated with muscle contraction (Reactome R-MMU-397014), biogenesis (Reactome R-MMU-1266738), rhabdomyosin contraction (Reactome R-MMU-390522), focal adhesion (KEGG PATHWAY mmu04510), and the ECM (Reactome R-MMU-1474244) (Table 3).

### 3.6 | Selection of Protein Interactions and Hub Genes in the IVDs of Aged Mice

We selected the top 100 high-degree nodes and assessed their relationships based on the combined STRING database score (filtering score, 900). A relationship was considered significant if the combined score between proteins or genes exceeded the set threshold in the STRING database; otherwise, the pair of genes or proteins was discarded (Figure 6). *Cox5a*, *Ndufs6*, *Ndufb9*, *Ttn*, *Ndufb6*, *Ndufb5*, *Atp5k*, *Tnnt3*, *Adamts2*, *Ndufb8*, *Uqcr11*, *Actn2*, *Atp5o*, *Uqcrb*, *Adamts3*, and *Ndufs4* were the top 16 hub genes.

## 4 | Discussion

Aging society and increasing economic pressure emphasize the need for developing new strategies for the early diagnosis and treatment of IVD degeneration, ultimately reducing the need for spinal fusion surgery [28]. Gene- and cell-based strategies effectively alleviate IVD degeneration and promote regeneration [29–32]. However, despite successful in vivo studies [33, 34], the clinical translation of these results is significantly hindered by differences in cell types among species and a lack of detailed understanding of the internal state of nucleus pulposus cells in the pathogenesis of IVD degeneration [35]. Therefore, identification of gene and cell mediators involved in the pathogenesis of IVD degeneration is urgently required to develop promising biological interventions in the near future.

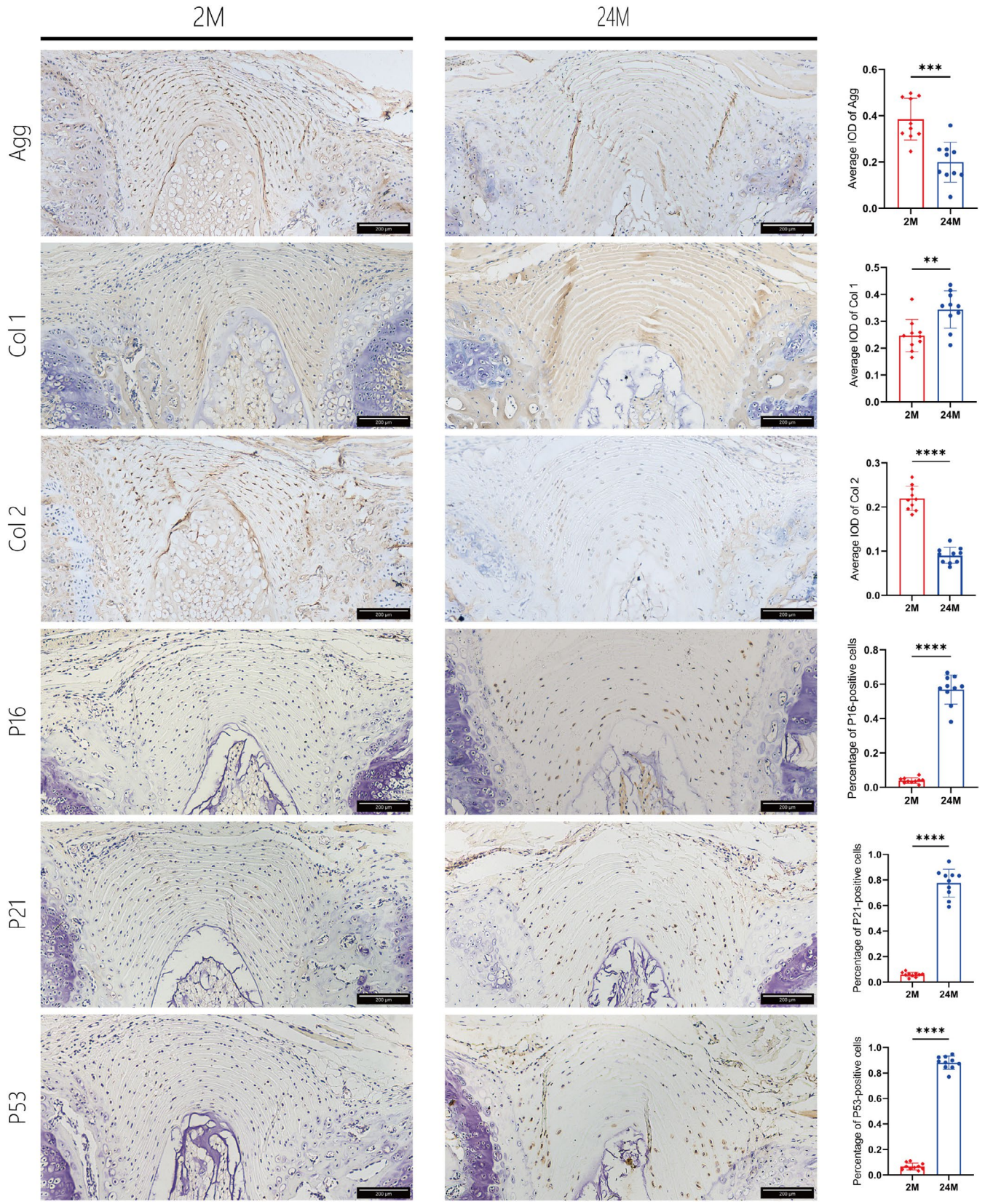


**FIGURE 2** | | Expression of biomarkers related to senescence and the extracellular matrix in IVDs. Immunohistochemical staining for P16, P21, and P53, and proportion of positively stained cells per high-power field to total cell count; immunohistochemical staining for Col1, Col2, and Agg, and average optical density; ****$p < 0.0001$, ***$p < 0.001$, **$p < 0.01$. Scale bar: 200 μm. IVD, intervertebral disk.

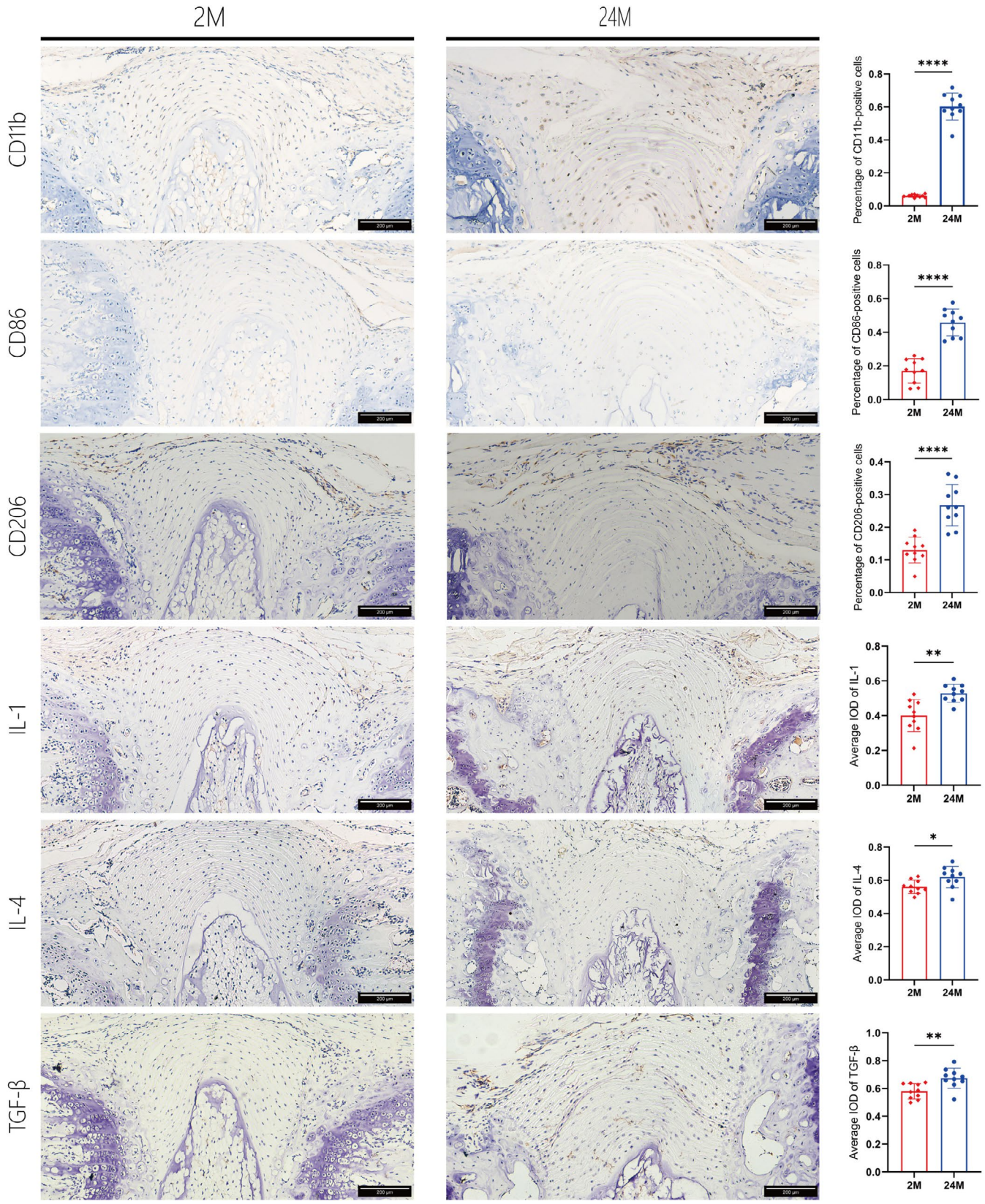


**FIGURE 3** | | Expression of macrophage, SASP, and inflammation-related markers in IVDs. Immunohistochemical staining for CD206, CD11b, and CD86, and proportion of positively stained cells per high-power field to total cell count; immunohistochemical staining for IL-1, IL-4, and TGF-β, and average optical density; *$p < 0.05$, **$p < 0.01$, ****$p < 0.0001$. Scale bar: 200 μm. SASP, senescence-associated secretory phenotype.

Aging is a major cause of the development and exacerbation of degenerative IVD disease [36]. Aging leads to degeneration and defects in all IVD tissues, which include reduced disk height, annular rupture, dehydration, and fibrosis of the nucleus pulposus, cartilage endplate destruction, and subchondral bone sclerosis [37]. However, the molecular mechanisms via which aging triggers regional pathological changes are not completely understood. Our results showed that the expression of aging-associated secretory components, IL-1, TGF-β, and the inflammatory factor, IL-4, in the IVDs of older mice was significantly higher than that in adult mice. Macrophage expression, irrespective of the type, also increased significantly compared with that in adult mice.

**TABLE 1** | Top five upregulated differential genes in elderly mice compared to adult mice.

| Gene | logFC | *p* | Adj. *p*-value |
|---|---|---|---|
| Srd5a2 | 7.62837718 | 4.33343E−05 | 0.010639542 |
| Slc38a5 | 7.514354023 | 3.78191E−05 | 0.010270325 |
| Gm47283 | 6.064202161 | 0.009563997 | 0.124236235 |
| Npy | 6.022405354 | 0.000759852 | 0.036114804 |
| Pcdh8 | 5.979980588 | 7.77444E−05 | 0.014413386 |

**TABLE 2** | Top five downregulated differential genes in elderly mice compared to adult mice.

| Gene | logFC | *p* | Adj. *p*-value |
|---|---|---|---|
| Kcna7 | −8.43776659645611 | 0.000446 | 0.028225 |
| Mmp9 | −8.42030207476387 | 0.030981 | 0.224615 |
| Panx3 | −8.19763370034756 | 0.001701 | 0.053171 |
| Myl10 | −7.4437989099349 | 1.62E−06 | 0.003817 |
| Bglap | −7.42303673902067 | 4.1E−05 | 0.010349 |

Inflammatory factors are key in the occurrence and development of IVD degeneration, which promotes catabolism, leading to ECM loss, cell apoptosis, and neurotrophic factor production [38].

Macrophages play multiple roles in the innate immune system, protecting the body from antigens. They clear foreign bodies in tissues, including pathogens, senescent cells, and their secreted products, and the byproducts of ECM degradation (such as collagen fragments) during tissue regeneration, which is critical for tissue repair [39–42]. The biological effects of macrophages on the IVD are mainly determined by their polarization state. M1 macrophages exacerbate disk degeneration by inhibiting cell proliferation and metabolic synthesis and promoting the secretion of pro-inflammatory mediators, whereas M2 macrophages attenuate disk degeneration by inhibiting ECM degradation and inflammatory responses [10]. Our previous study using an RheBcKO mouse model of IVD degeneration showed that promoting M2 polarization of macrophages can mitigate the progression of disk degeneration [43].

Ling et al. used single-cell RNA sequencing technology to study the molecular programs, lineage progression patterns, and cell communication pathways of nucleus pulposus cells in different grades of IVD degeneration in patients who underwent discectomy. They found that the polarization of M1 and M2 macrophages was in a dynamic state, and that the nucleus pulposus cells in the late stage of degeneration were mainly composed of subtypes related to inflammation and endoplasmic reticulum responses and fibrocartilage activity [44]. Macrophages participate in ECM degradation and remodeling by producing matrix metalloproteinases and enzymes belonging to a disintegrin and metalloproteinase domain with

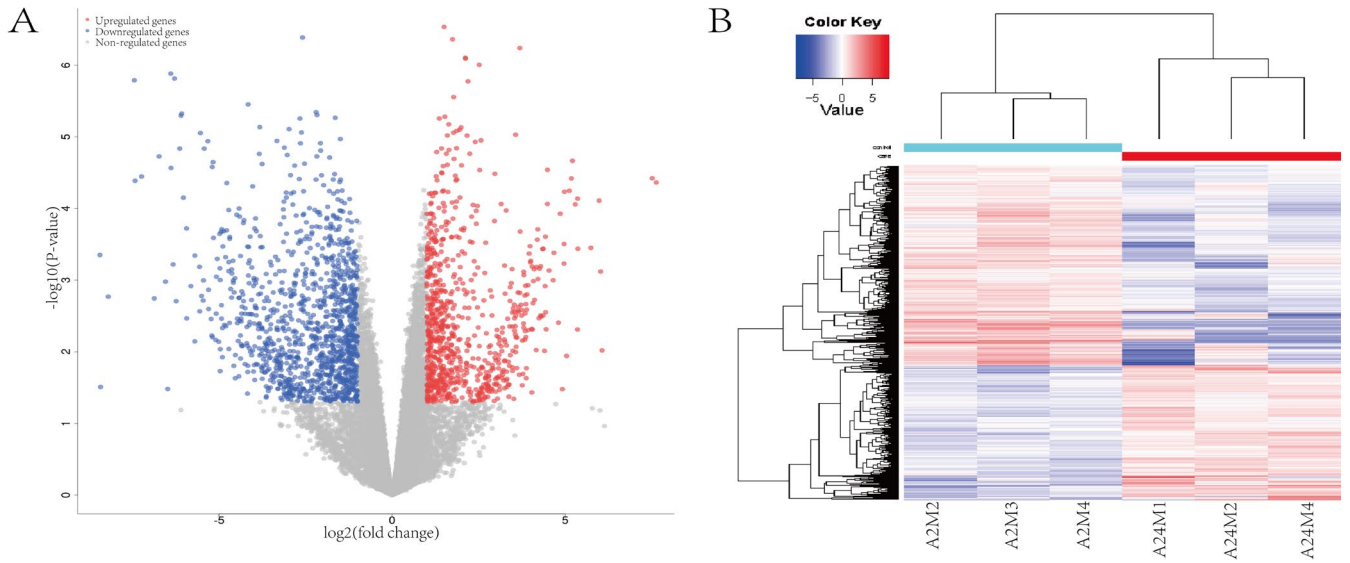


**FIGURE 4** | | Volcano plot and clustering chart of differentially expressed genes related to aging. (A) Volcano plot. Horizontal axis, log2 value of fold difference; vertical axis, negative logarithm *p*-value. Red and blue points represent differentially expressed genes with upregulated and downregulated expression, respectively; gray points represent genes with no significant differences in expression during aging; (B) Clustering chart.

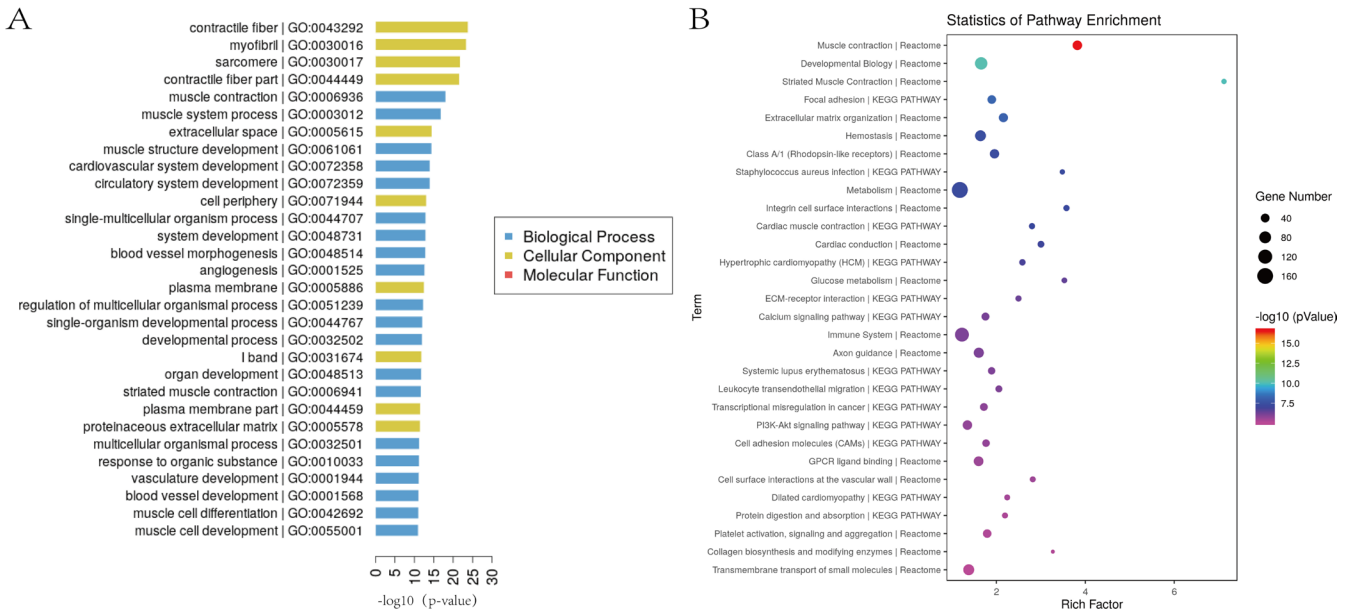


**FIGURE 5** | | GO enrichment statistical chart and pathway enrichment factor chart. (A) Statistical chart of the top 30 GO entries; (B) Pathway enrichment factor chart. GO, Gene Ontology.

**TABLE 3** | Top five enriched pathways.

| Term | Database | ID | Input number | Background number | *p* |
|---|---|---|---|---|---|
| Muscle contraction | Reactome | R-MMU-397014 | 48 | 154 | 2.76532E−17 |
| Developmental biology | Reactome | R-MMU-1266738 | 89 | 658 | 8.22995E−11 |
| Striated muscle contraction | Reactome | R-MMU-390522 | 18 | 31 | 9.9346E−11 |
| Focal adhesion | KEGG | mmu04510 | 39 | 203 | 6.36967E−09 |
| Extracellular matrix organization | Reactome | R-MMU-1474244 | 44 | 250 | 7.27067E−09 |

thrombospondin motif (ADAMTS) family [45, 46]. Ndufs6 is evidently associated with P53/P21 upregulation, showing a close association with senescence, and ADAMTS2 plays an important role in the specific induction of macrophages [47, 48].

Cellular anabolic and catabolic activities maintain the integrity and health of the IVD by producing ECM components and chemicals responsible for matrix degradation and cell survival, which are energy-intensive processes. The disk microenvironment, which includes inflammatory cascades and mechanical stress, contributes significantly to cellular metabolic activities and aging [48, 49]. However, the clearing of senescent cells alleviates age-related hydrolysis of the IVD protein matrix; this indicates that senescent cells produce inflammatory cytokines and catabolic proteases, the levels of which increase with IVD aging, supporting the causal relationship between cellular senescence and age-related IVD degeneration [20]. Collectively, these findings will assist in the early diagnosis and treatment of degeneration during human IVD aging.

There is a correlation among IVD macrophage number, inflammatory phenotype, and disease severity [47]; however, data confirming the causal role of macrophages in disk degeneration, which is crucial for understanding the progression of IVD degeneration during aging, are lacking.

In conclusion, the IVD height decreased, while the expression of both aging-related secretory phenotypes and macrophage polarization markers increased significantly with increasing age and disk senescence in mice. Aged mice showed upregulated expression of *Kcna7*, *Mmp9*, *Panx3*, *Myl10*, and *Bglap* and downregulated expression of *Srd5a2*, *Slc38a5*, *Gm47283*, *Npy*, and *Pcdh8*. Differential senescence gene–protein network interaction analysis revealed the following hub genes: *Cox5a*, *Ndufs6*, *Ndufb9*, *Ttn*, *Ndufb6*, *Ndufb5*, *Atp5k*, *Tnnt3*, *Adamts2*, *Ndufb8*, *Uqcr11*, *Actn2*, *Atp5o*, *Uqcrb*, *Adamts3*, and *Ndufs4*. Therefore, the identification of common features of pathological aging and degeneration of IVD function in the future is crucial for guiding new treatments. However, to the best of our knowledge, no systematic study has evaluated the cellular aging phenomenon in mouse IVDs. Here, (a) important experimental evidence for studying changes in macrophages in aging IVDs, (b) related hug genes, and (c) a new research content for elucidating the pathogenesis of age-related degenerative disk diseases are provided.

Nonetheless, this study has some limitations. First, male mice was used, and no further investigation was conducted in female

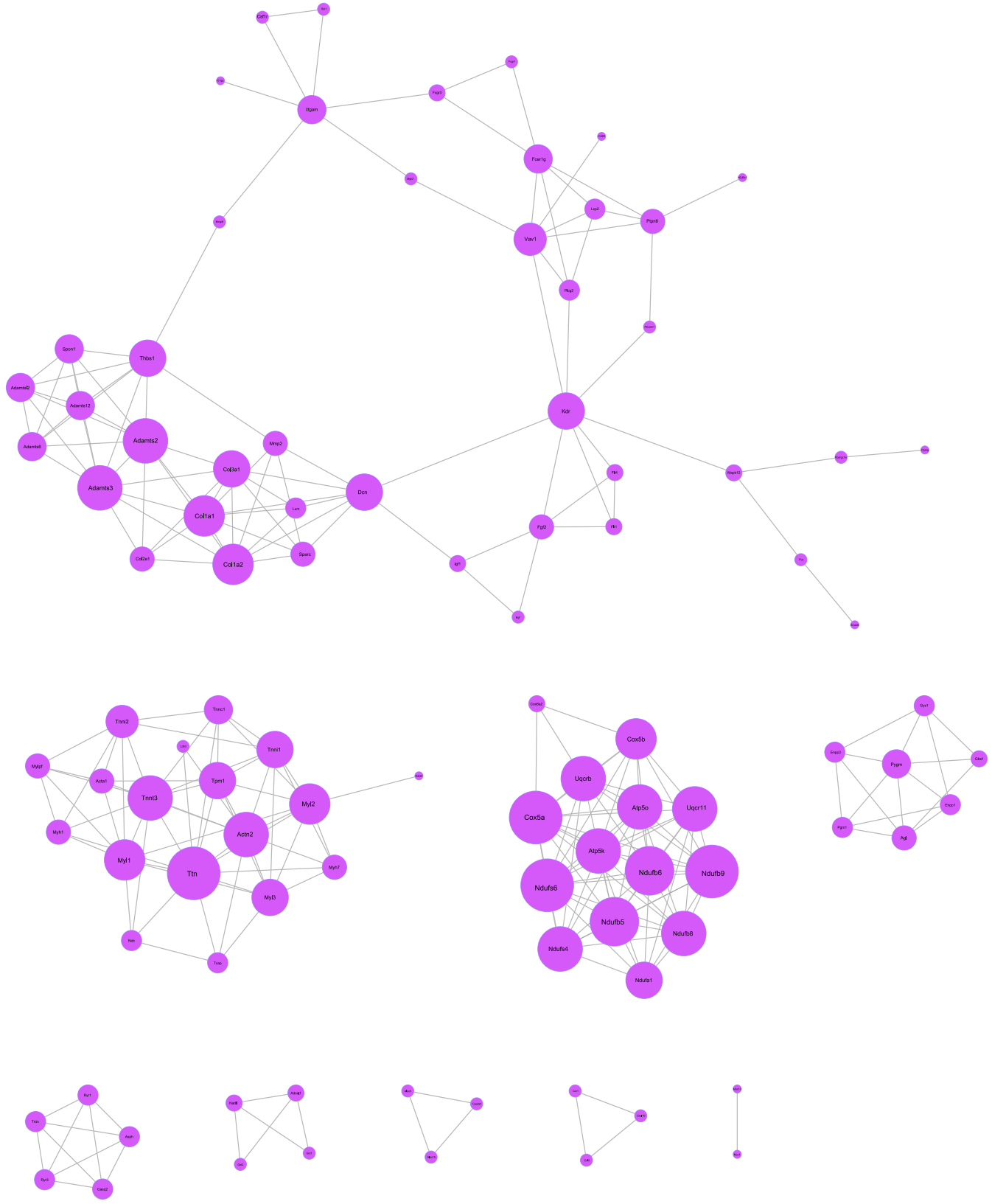


**FIGURE 6** | | Protein–protein interaction network in aging mouse IVDs. Nodes represent hub genes and edges represent protein interactions. The size represents the rating, and the higher the score, the larger the node.

mice, which may have introduced a bias in the experimental results. Second, macrophage polarization and aging-associated secretory phenotype increased significantly, indicating their role in the aging process in the IVD; however, further studies are required to investigate their relationship in detail. Last, analysis of the differential gene–protein network interaction related

to aging resulted in the identification of hub genes. However, further validation is required to confirm the role of hub genes in macrophage changes during aging.


### Acknowledgments

We thank Editage (www.editage.cn) for English language editing.


### Conflicts of Interest

The authors declare no conflicts of interest.

### References


1. Global Burden of Disease Study 2013 Collaborators, "Global, Regional, and National Incidence, Prevalence, and Years Lived With Disability for 301 Acute and Chronic Diseases and Injuries in 188 Countries, 1990–2013: A Systematic Analysis for the Global Burden of Disease Study 2013," *Lancet* 386, no. 10159 (2015): 743–800, https://doi.org/10.1016/S0140-6736(15)60692-4.

2. X. Luo, R. Pietrobon, S. X. Sun, G. G. Liu, and L. Hey, "Estimates and Patterns of Direct Health Care Expenditures Among Individuals With Back Pain in the United States," *Spine (Phila Pa 1976)* 29, no. 1 (2004): 79–86, https://doi.org/10.1097/01.BRS.0000105527.13866.0F.

3. A. Kędra, M. Plandowska, P. Kędra, and D. Czaprowski, "Physical Activity and Low Back Pain in Children and Adolescents: A Systematic Review," *European Spine Journal* 30, no. 4 (2021): 946–956, https://doi.org/10.1007/s00586-020-06575-5.

4. I. Calvo-Muñoz, A. Gómez-Conesa, and J. Sánchez-Meca, "Prevalence of Low Back Pain in Children and Adolescents: A Meta-Analysis," *BMC Pediatrics* 13 (2013): 14, https://doi.org/10.1186/1471-2431-13-14.

5. D. Sakai and G. B. Andersson, "Stem Cell Therapy for Intervertebral Disc Regeneration: Obstacles and Solutions," *Nature Reviews Rheumatology* 11, no. 4 (2015): 243–256, https://doi.org/10.1038/nrrheum.2015.13.

6. H. Yang, H. Liu, Z. Li, et al., "Low Back Pain Associated With Lumbar Disc Herniation: Role of Moderately Degenerative Disc and Annulus Fibrous Tears," *International Journal of Clinical and Experimental Medicine* 8, no. 2 (2015): 1634–1644.

7. T. Takada, K. Nishida, M. Doita, H. Miyamoto, and M. Kurosaka, "Interleukin-6 Production Is Upregulated by Interaction Between Disc Tissue and Macrophages," *Spine* 29, no. 10 (2004): 1089–1092. discussion 1093, https://doi.org/10.1097/00007632-200405150-00007.

8. G. G James, K. A. Sluka, L. Blomster, et al., "Macrophage Polarization Contributes to Local Inflammation and Structural Change in the Multifidus Muscle After Intervertebral Disc Injury," *European Spine Journal* 27, no. 8 (2018): 1744–1756, https://doi.org/10.1007/s00586-018-5652-7.

9. M. F. Shamji, L. A. Setton, W. Jarvis, et al., "Proinflammatory Cytokine Expression Profile in Degenerated and Herniated Human Intervertebral Disc Tissues," *Arthritis and Rheumatism* 62, no. 7 (2010): 1974–1982, https://doi.org/10.1002/art.27444.

10. X. C. Li, S. J. Luo, W. Fan, et al., "Macrophage Polarization Regulates Intervertebral Disc Degeneration by Modulating Cell Proliferation, Inflammation Mediator Secretion, and Extracellular Matrix Metabolism," *Frontiers in Immunology* 13 (2022): 922173, https://doi.org/10.3389/fimmu.2022.922173.

11. L. A. Nasto, K. Ngo, A. S. Leme, et al., "Investigating the Role of DNA Damage in Tobacco Smoking-Induced Spine Degeneration," *Spine Journal* 14, no. 3 (2014): 416–423, https://doi.org/10.1016/j.spinee.2013.08.034.

12. C. H. Moon, L. Jacobs, J. H. Kim, et al., "Part 2: Quantitative Proton T2 and Sodium Magnetic Resonance Imaging to Assess Intervertebral Disc Degeneration in a Rabbit Model," *Spine (Phila Pa 1976)* 37, no. 18 (2012): E1113–E1119, https://doi.org/10.1097/BRS.0b013e3182583447.

13. D. Samartzis, J. Karppinen, D. Chan, K. D. Luk, and K. M. Cheung, "The Association of Lumbar Intervertebral Disc Degeneration on Magnetic Resonance Imaging With Body Mass Index in Overweight and Obese Adults: A Population-Based Study," *Arthritis and Rheumatism* 64, no. 5 (2012): 1488–1496, https://doi.org/10.1002/art.33462.

14. P. Silwal, A. M. Nguyen-Thai, H. A. Mohammad, et al., "Cellular Senescence in Intervertebral Disc Aging and Degeneration: Molecular Mechanisms and Potential Therapeutic Opportunities," *Biomolecules* 13, no. 4 (2023): 686, https://doi.org/10.3390/biom13040686.

15. N. Boos, S. Weissbach, H. Rohrbach, C. Weiler, K. F. Spratt, and A. G. Nerlich, "Classification of Age-Related Changes in Lumbar Intervertebral Discs: 2002 Volvo Award in Basic Science," *Spine (Phila Pa 1976)* 27, no. 23 (2002): 2631–2644, https://doi.org/10.1097/00007632-200212010-00002.

16. C. Kilkenny, W. J. Browne, I. C. Cuthill, M. Emerson, and D. G. Altman, "Improving Bioscience Research Reporting: The ARRIVE Guidelines for Reporting Animal Research," *PLoS Biology* 8, no. 6 (2010): e1000412.

17. G. K. Smyth, "Linear Models and Empirical Bayes Methods for Assessing Differential Expression in Microarray Experiments," *Statistical Applications in Genetics and Molecular Biology* 3, no. 1 (2004): 1–25, https://doi.org/10.2202/1544-6115.1027.

18. J. Wu, X. Mao, T. Cai, J. Luo, and L. Wei, "KOBAS Server: A Web-Based Platform for Automated Annotation and Pathway Identification," *Nucleic Acids Research* 34 (2006): W720–W724, https://doi.org/10.1093/nar/gkl167.

19. M. L. Ji, H. Jiang, X. J. Zhang, et al., "Preclinical Development of a microRNA-Based Therapy for Intervertebral Disc Degeneration," *Nature Communications* 9, no. 1 (2018): 5051, https://doi.org/10.1038/s41467-018-07360-1.

20. P. Patil, Q. Dong, D. Wang, et al., "Systemic Clearance of p16INK4a-Positive Senescent Cells Mitigates Age-Associated Intervertebral Disc Degeneration," *Aging Cell* 18, no. 3 (2019): e12927, https://doi.org/10.1111/acel.12927.

21. K. Ngo, P. Patil, S. J. McGowan, et al., "Senescent Intervertebral Disc Cells Exhibit Perturbed Matrix Homeostasis Phenotype," *Mechanisms of Ageing and Development* 166 (2017): 16–23, https://doi.org/10.1016/j.mad.2017.08.007.

22. S. Lee, S. H. Jang, M. Suzuki-Narita, S. Gregoire, M. Millecamps, and L. S. Stone, "Voluntary Running Attenuates Behavioural Signs of Low Back Pain: Dimorphic Regulation of Intervertebral Disc Inflammation in Male and Female SPARC-Null Mice," *Osteoarthritis and Cartilage* 30, no. 1 (2022): 110–123, https://doi.org/10.1016/j.joca.2021.06.014.

23. Y. Y Zhou, P. Nan, C. Li, et al., "Upregulation of MTA1 in Colon Cancer Drives A CD8+ T Cell-Rich but Classical Macrophage-Lacking Immunosuppressive Tumor Microenvironment. Front," *Oncologia* 12 (2022): 825783, https://doi.org/10.3389/fonc.2022.825783.

24. Y. Yokozeki, A. Kawakubo, M. Miyagi, et al., "Reduced TGF-β Expression and CD206-Positive Resident Macrophages in the Intervertebral Discs of Aged Mice," *BioMed Research International* 2021 (2021): 7988320, https://doi.org/10.1155/2021/7988320.

25. C. Ribeiro-Machado, S. G. Santos, I. A. Amaral, et al., "Macrophage-Based Therapy for Intervertebral Disc Herniation: Preclinical Proof-Of-Concept," *npj Regenerative Medicine* 8, no. 1 (2023): 34, https://doi.org/10.1038/s41536-023-00309-z.

26. S. He and N. E. Sharpless, "Senescence in Health and Disease," *Cell* 169, no. 6 (2017): 1000–1011, https://doi.org/10.1016/j.cell.2017.05.015.

27. B. C. Capell, A. M. Drake, J. Zhu, et al., "MLL1 Is Essential for the Senescence-Associated Secretory Phenotype," *Genes & Development* 30, no. 3 (2016): 321–336, https://doi.org/10.1101/gad.271882.115.

28. Z. Liu, J. Li, M. Hu, et al., "The Optimal Timing of Hydrogel Injection for Treatment of Intervertebral Disc Degeneration: Quantitative Analysis Based on T1ρ MR Imaging," *Spine (Phila Pa 1976)* 45, no. 22 (2020): E1451–E1459, https://doi.org/10.1097/BRS.0000000000003667.

29. S. Chen, M. Luo, H. Kou, G. Shang, Y. Ji, and H. Liu, "A Review of Gene Therapy Delivery Systems for Intervertebral Disc Degeneration," *Current Pharmaceutical Biotechnology* 21, no. 3 (2020): 194–205, https://doi.org/10.2174/1389201020666191024171618.

30. Y. Takeoka, T. Yurube, and K. Nishida, "Gene Therapy Approach for Intervertebral Disc Degeneration: An Update," *Neurospine* 17, no. 1 (2023): 3–14, https://doi.org/10.14245/ns.2040042.021.

31. S. Vedicherla and C. T. Buckley, "Cell-Based Therapies for Intervertebral Disc and Cartilage Regeneration- Current Concepts, Parallels, and Perspectives," *Journal of Orthopaedic Research* 35, no. 1 (2017): 8–22, https://doi.org/10.1002/jor.23268.

32. D. Oehme, T. Goldschlager, P. Ghosh, J. V. Rosenfeld, and G. Jenkin, "Cell-Based Therapies Used to Treat Lumbar Degenerative Disc Disease: A Systematic Review of Animal Studies and Human Clinical Trials," *Stem Cells International* 2015 (2015): 946031, https://doi.org/10.1155/2015/946031.

33. Y. Gan, P. Li, L. Wang, et al., "An Interpenetrating Network-Strengthened and Toughened Hydrogel That Supports Cell-Based Nucleus Pulposus Regeneration," *Biomaterials* 136 (2017): 12–28, https://doi.org/10.1016/j.biomaterials.2017.05.017.

34. G. Feng, Z. Zhang, M. Dang, et al., "Injectable Nanofibrous Spongy Microspheres for NR4A1 Plasmid DNA Transfection to Reverse Fibrotic Degeneration and Support Disc Regeneration," *Biomaterials* 131 (2017): 86–97, https://doi.org/10.1016/j.biomaterials.2017.03.029.

35. M. R. McCann and C. A. Séguin, "Notochord Cells in Intervertebral Disc Development and Degeneration," *Journal of Developmental Biology* 4, no. 1 (2016): 3, https://doi.org/10.3390/jdb4010003.

36. O. Alvarez-Garcia, T. Matsuzaki, M. Olmer, K. Masuda, and M. K. Lotz, "Age-Related Reduction in the Expression of FOXO Transcription Factors and Correlations With Intervertebral Disc Degeneration," *Journal of Orthopaedic Research* 35, no. 12 (2017): 2682–2691, https://doi.org/10.1002/jor.23583.

37. M. J. Silva and N. Holguin, "Aging Aggravates Intervertebral Disc Degeneration by Regulating Transcription Factors Toward Chondrogenesis," *FASEB Journal* 34, no. 2 (2020): 1970–1982, https://doi.org/10.1096/fj.201902109R.

38. F. J. Lyu, H. Cui, H. Pan, et al., "Painful Intervertebral Disc Degeneration and Inflammation: From Laboratory Evidence to Clinical Interventions," *Bone Research* 9, no. 1 (2021): 7, https://doi.org/10.1038/s41413-020-00125-x.

39. A. I. Tauber, "Metchnikoff and the Phagocytosis Theory," *Nature Reviews Molecular Cell Biology* 4, no. 11 (2003): 897–901, https://doi.org/10.1038/nrm1244.

40. F. Prattichizzo, M. Bonafè, F. Olivieri, and C. Franceschi, "Senescence Associated Macrophages and "Macroph-Aging": Are They Pieces of the Same Puzzle?," *Aging (Albany NY)* 8, no. 12 (2016): 3159–3160, https://doi.org/10.18632/aging.101133.

41. J. Zhou, Z. Tang, S. Gao, C. Li, Y. Feng, and X. Zhou, "Tumor-Associated Macrophages: Recent Insights and Therapies," *Frontiers in Oncology* 10 (2020): 188, https://doi.org/10.3389/fonc.2020.00188.

42. M. L. Thorseth, M. Carretta, C. Jensen, et al., "Uncovering Mediators of Collagen Degradation in the Tumor Microenvironment," *Matrix Biology Plus* 13 (2022): 100101, https://doi.org/10.1016/j.mbplus.2022.100101.

43. X. C. Li, W. Wang, C. Jiang, et al., "CD206+ M2-Like Macrophages Protect Against Intervertebral Disc Degeneration Partially by Targeting R-Spondin-2," *Osteoarthritis and Cartilage* 32, no. 1 (2024): 66–81, https://doi.org/10.1016/j.joca.2023.09.010.

44. Z. Ling, Y. Liu, Z. Wang, et al., "Single-Cell RNA-Seq Analysis Reveals Macrophage Involved in the Progression of Human Intervertebral Disc Degeneration," *Frontiers in Cell and Development Biology* 9 (2021): 833420, https://doi.org/10.3389/fcell.2021.833420.

45. J. Koroth, E. O. Buko, R. Abbott, et al., "Macrophages and Intervertebral Disc Degeneration," *International Journal of Molecular Sciences* 24, no. 2 (2023): 1367, https://doi.org/10.3390/ijms24021367.

46. C. Wang, S. Gonzales, H. Levene, W. Gu, and C. Y. Huang, "Energy Metabolism of Intervertebral Disc Under Mechanical Loading," *Journal of Orthopaedic Research* 31, no. 11 (2013): 1733–1738, https://doi.org/10.1002/jor.22436.

47. Y. Zhang, L. Guo, S. Han, et al., "Adult Mesenchymal Stem Cell Ageing Interplays With Depressed Mitochondrial Ndufs6," *Cell Death & Disease* 11, no. 12 (2020): 1075, https://doi.org/10.1038/s41419-020-03289-w.

48. T. P. Hofer, M. Frankenberger, J. Mages, et al., "Tissue-Specific Induction of ADAMTS2 in Monocytes and Macrophages by Glucocorticoids," *Journal of Molecular Medicine (Berlin, Germany)* 86, no. 3 (2008): 323–332, https://doi.org/10.1007/s00109-007-0284-0.

49. E. S. Silagi, I. M. Shapiro, and M. V. Risbud, "Glycosaminoglycan Synthesis in the Nucleus Pulposus: Dysregulation and the Pathogenesis of Disc Degeneration," *Matrix Biology* 71–72 (2018): 368–379, https://doi.org/10.1016/j.matbio.2018.02.025.